Acta Crystallographica Section B
Structural Science
ISSN 0108-7681

Structural phase transitions of HfV_2 at low temperatures

Yusheng Zhao,[a]* Fuming Chu,[b] Robert B. Von Dreele[a] and Qing Zhu[c]

[a]LANSCE Division, Los Alamos National Laboratory, Los Alamos, NM 87545, USA, [b]MST Division, Los Alamos National Laboratory, Los Alamos, NM 87545, USA, and [c]Physics Department, Brookhaven National Laboratory, Upton, NY 11973, USA

Correspondence e-mail: yzhao@lanl.gov

Received 1 November 1999
Accepted 7 March 2000

We report a high-resolution synchrotron X-ray powder diffraction study on HfV_2, hafnium divanadium, at low temperatures. In this work we show, for the first time, a complete sequence of structural phase transitions of HfV_2 from cubic ($Fd3m$) to tetragonal ($I4_1/amd$) to orthorhombic ($Imma$) in succession as temperature decreases. Peak splitting and extra diffraction peaks owing to lattice distortion can be clearly distinguished for the low-symmetry phases. The atomic positions and lattice parameters were obtained by Rietveld refinement. The bond lengths and angles of the HfV_2 crystal structure at the low-symmetry phases were correctly determined from the structure refinement. The face-centered cubic ($Fd3m$) unit cell (Z = 24) transforms to a body-centered tetragonal ($I4_1/amd$) phase with a 45° rotation relative to the cubic cell and with a reduced number of atoms (Z = 12) in the unit cell at a temperature of T = 112 K. The orthorhombic phase occurs at T = 102 K and it keeps the body-centered symmetry ($Imma$) and Z = 12 in the unit cell. The refinement results indicate that there may be a small amount of untransformed cubic phase left over in the lower symmetry phases. The abnormal thermal contraction of both tetragonal phase and orthorhombic phase marks the significance of structural change in HfV_2.

1. Introduction

Topologically close-packed (TCP) intermetallic compounds are promising candidates for high-temperature structural studies as ordered forms of *f.c.c.*, *b.c.c.* and *h.c.p.* metals because of their intrinsic properties of low density and high melting temperature. In the group of TCP intermetallics, Laves phases constitute the single largest group, forming ~27% of the population. The crystal structure of Laves phases can be either a cubic C15 ($MgCu_2$), hexagonal C14 ($MgZn_2$) or dihexagonal C36 ($MgNi_2$). The C15 phase has more than 1000 binary and ternary forms among the three types of Laves phases. Uniquely, only HfV_2 and UMn_2 C15 Laves phases exhibit peculiar physical and mechanical properties, including: temperature-induced structural phase transformations (Lawson & Zachariasen, 1972; Hafstrom *et al.*, 1978; Lawson *et al.*, 1987; Chu *et al.*, 1996), anomalous thermal softening of elastic properties (Finlayson *et al.*, 1978; Balankin & Skorov, 1982; Chu *et al.*, 1994), mechanical deformation twinning in low temperatures (Livingston & Hall, 1990; Chu & Pope, 1993) and the highest superconducting temperature (T_{sc} = 9.6 K) among intermetallics (Chu *et al.*, 1996). For more than three decades, continuous efforts have been made to understand the observed anomalies, reveal driving mechan-

isms and illustrate relationships between unusual physical properties.

Crystallography holds one of the most important keys to elucidate the nature of crystal structure instability and phase transitions in HfV_2. To date, there is a lack of credible high-quality data of the crucial structural information at low temperatures. The low-temperature phase of HfV_2 has been initially identified to be an orthorhombic structure with the space group *Imm*2 (Lawson & Zachariasen, 1972). Recently, it has been refined as an *Imma* phase (Parsons *et al.*, 1998), with neutron diffraction data. Many researchers have postulated the existence of a tetragonal phase between cubic and orthorhombic structures, however, it has never been observed experimentally. The present study employs high-resolution synchrotron X-ray powder diffraction and Rietveld refinement techniques to study the crystallography of HfV_2 at low temperatures. We concentrate on three critical issues:

(i) to search for the existence of the long speculated tetragonal phase,

(ii) to provide accurate and precise atomic positions of the low-symmetry crystal structure, and

(iii) to study the process of crystal structure instability and the nature of structural phase transformations of HfV_2.

2. Experimental

High-resolution diffraction experiments were conducted using synchrotron X-ray powder diffraction at beamline X7A of the National Synchrotron Light Source (NSLS). The polycrystalline sample of HfV_2 having the C15 cubic structure was prepared by melting a stoichiometric ratio of the constituents in a conventional inert atmosphere arc furnace. Arc-melted buttons were made using elemental Hf and V with nominal purities of 99.97 and 99.9 at % (Alfa Aesar, A. Johnson Matthey Company) and the sample was annealed under high vacuum at 1500 K for 120 h. The diffraction data were collected by a scintillation detector in the angular dispersive mode over a 2θ interval from 5 to 60° with a scan step of 0.005° at a monochromatic wavelength of $\lambda = 0.7508$ Å. The combination of high instrumental resolution, very short wavelength and wide *d*-spacing coverage down to 0.75 Å allows accurate and precise structure refinement. Low temperatures on the sample were achieved by a cryostat attached to the diffractometer and were measured stable to within ±0.1 K. The diffraction patterns at different temperatures were analyzed by the Rietveld whole profile refinement method (Rietveld, 1969) using the computer program *GSAS* (Larson & Von Dreele, 1994). The Rietveld method permits the refinement of the unit-cell dimensions and atomic positions in the crystal structure simultaneously. The fitting of the diffraction profile is achieved by a least-squares method of minimizing the differences between the observed pattern and the calculated pattern. There were small secondary diffraction peaks revealed by the X-ray diffraction data indicating minor impurities in the sample. These low-intensity secondary peaks, being a cubic phase with a lattice parameter $a = 12.045$ Å, were excluded in the refinement procedure. Plotted in Fig. 1 are the refinement results for four different temperatures and the general agreement of the observed and synthetic diffraction pattern indicates the goodness of the structural models for different phases.

The cubic phase of HfV_2 with space group $Fd3m$ was observed for temperatures from 200 K down to 112.5 K. The diffraction peaks of the cubic phase are all isolated singlets with very fine peak widths (full-width at half maximum, FWHM $\Delta\theta/\theta \simeq 10^{-3}$). The diffraction pattern measured between 110 and 105 K showed apparent peak splitting and most singlets become doublets. The diffraction pattern observed below $T = 100$ K revealed further splitting of doublet peaks and relative intensities were also correspondingly changed. This observation suggests that there are two successive structural phase transformations occurring in HfV_2 within this temperature interval. A series of short scans (Fig. 2) focused on particular diffraction peaks were then performed with a temperature increment of $\Delta T = 2.5$ K for a temperature interval of 100 to 115 K. The $(211)_T$ peak is asymmetric at $T =$ 110 and 107.5 K (Fig. 2), suggesting that there is a coexistence of cubic and tetragonal phases over a narrow region. The phase boundaries were thus determined clearly at $T_{C1} = 112$ K

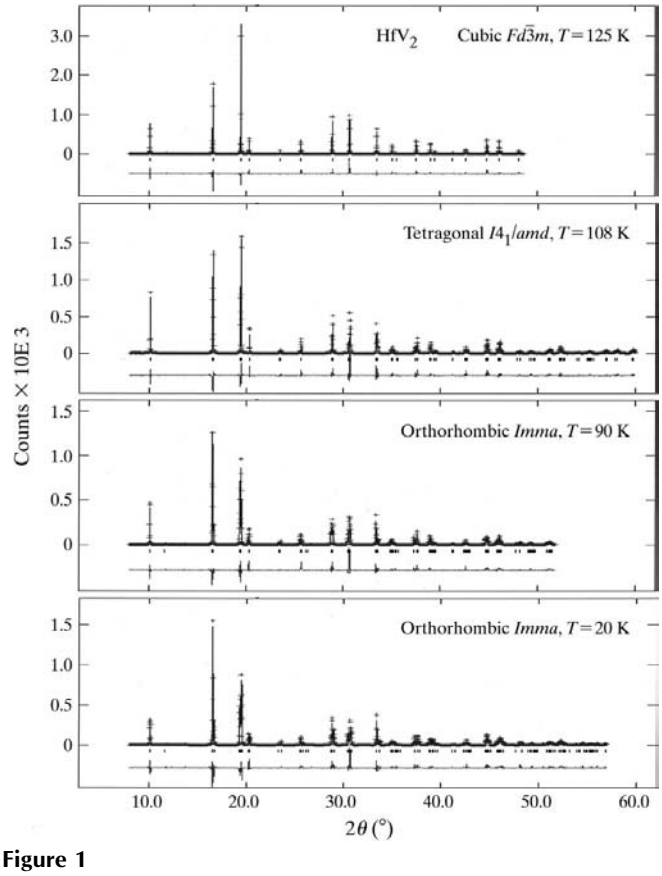

Figure 1
Refinement results of long-scan diffraction patterns observed at four different temperatures. The structural phases and experimental temperatures are labeled for each diffraction pattern. The diffraction peak positions are indicated by small tick-marks and the bottom curve is an illustration of the difference between observed (crosses) and calculated diffraction patterns.

for cubic to tetragonal and at T_{C2} = 102 K for tetragonal to orthorhombic phase transitions.

3. Discussion

3.1. Transition from cubic *Fd*3*m* to tetragonal $I4_1/amd$

Group theory indicates that there are five possible non-isomorphic subgroups for the cubic *Fd*3*m* phase: they are $I4_1/amd$, *R*3*m*, *Fd*3, $F4_132$, *F*43*m*, respectively. The last three space groups are still of the cubic symmetry and peak splitting should not occur in these phases. Therefore, these three are not possible subgroups of the cubic *Fd*3*m* for the observed phase transition at *T* = 112 K. The space groups of *R*3*m* and $I4_1/amd$ are rhombohedral and tetragonal phases, respectively, which should show significant differences for the diffraction peaks with respect to their splitting and intensities.

A close examination of the long-scan diffraction pattern observed at *T* = 107.5 K reveals that the peak splitting occurs only for those peaks with indexes $h = k \neq l$ and $h \neq k = l$ in the cubic phase, while the peaks with index $h = k = l$ in the cubic phase did not show peak splitting. For those doublets in the new phase, one peak at the lower *d*-spacing has twice the intensity as the other one at the higher *d*-spacing. The above observations excluded rhombohedral *R*3*m* as a possible candidate, of which the singlet with index $h = k = l$ in the cubic phase should split and there should be a ratio of 1/3 for the new doublet. The observed diffraction for the tetragonal phase at *T* = 107.5 K must belong to the long speculated tetragonal phase $I4_1/amd$. Further refinements using the Rietveld technique to adjust atomic positions and lattice parameters (Table 1) derived showed an excellent match of

Table 1
Structural parameters and unit-cell dimensions refined from long-scan diffraction data.

	Cubic		Tetragonal		Orthorhombic		
	(*Fd*3*m*)		($I4_1/amd$)		(*Imma*)		
	T = 125 K		*T* = 107.5 K		*T* = 90 K		*T* = 20 K
Atom	Hf	V	Hf	V	Hf	V(2)	V(1)
M (Wyckoff)	8(*b*)	16(*c*)	4(*b*)	8(*c*)	4(*e*)	4(*d*)	4(*a*)
x	3/8	0	0	0	0	1/4	0
y	3/8	0	1/4	0	1/4	3/4	0
z	3/8	0	3/8	0	3/8 + *w*	1/4	0
a	7.3752 (1)		5.2071 (1)		5.1910 (1)		5.1735 (1)
b					5.2124 (1)		5.2211 (1)
c			7.4014 (2)		7.4175 (1)		7.4320 (2)
'Cubic' (%)	100		9.7 (3)		11.7 (7)		12.8 (6)
χ^2	10.2		7.9		10.6		10.1

M represents multiplicity; *w* = 0.000253 (40) for *T* = 90 K and *w* = −0.000257 (30) for *T* = 20 K; 'cubic' indicates the phase fraction of the 'untransformed cubic' phase; χ^2 is the goodness-of-fit (see *GSAS* manual for definition; Larson & Von Dreele, 1994).

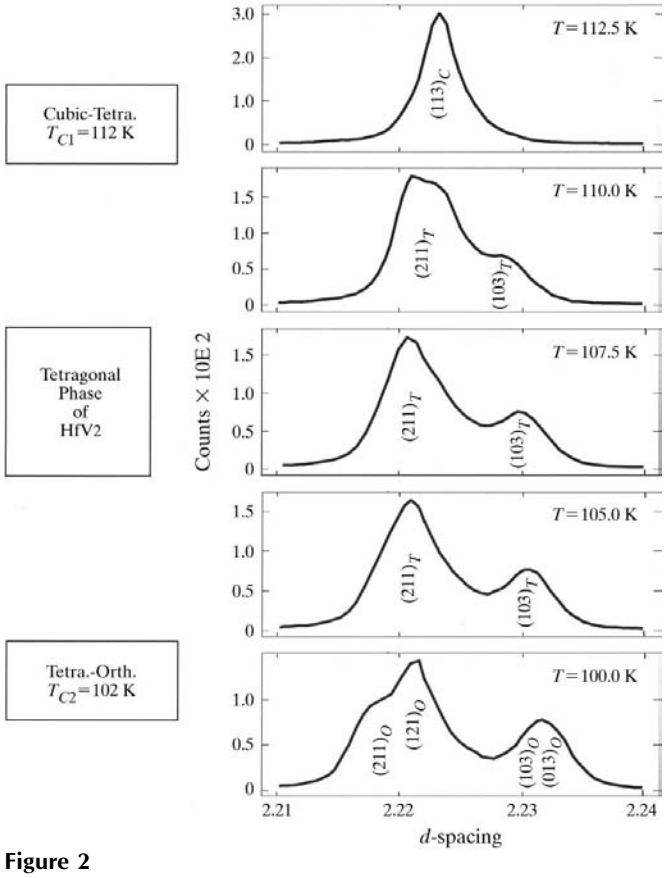

Figure 2
Fine-step (small temperature interval) scans focus on particular diffraction peaks due to lattice distortion to reveal the cubic–tetrahedral–orthorhombic phase transitions.

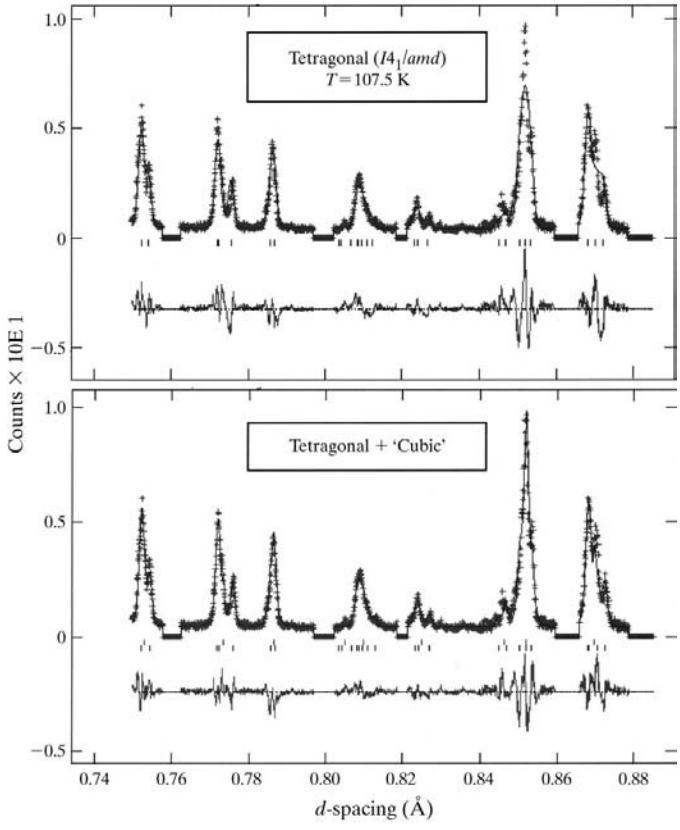

Figure 3
Refinement details at low *d*-spacing (high 2θ angle) for the diffraction pattern collected at *T* = 107.5 K. The top diagram shows the refinement results of the pure tetragonal ($I4_1/amd$) phase, while the bottom diagram has the 'untransformed cubic' component involved in the refinement (as indicated by the tick-marks).

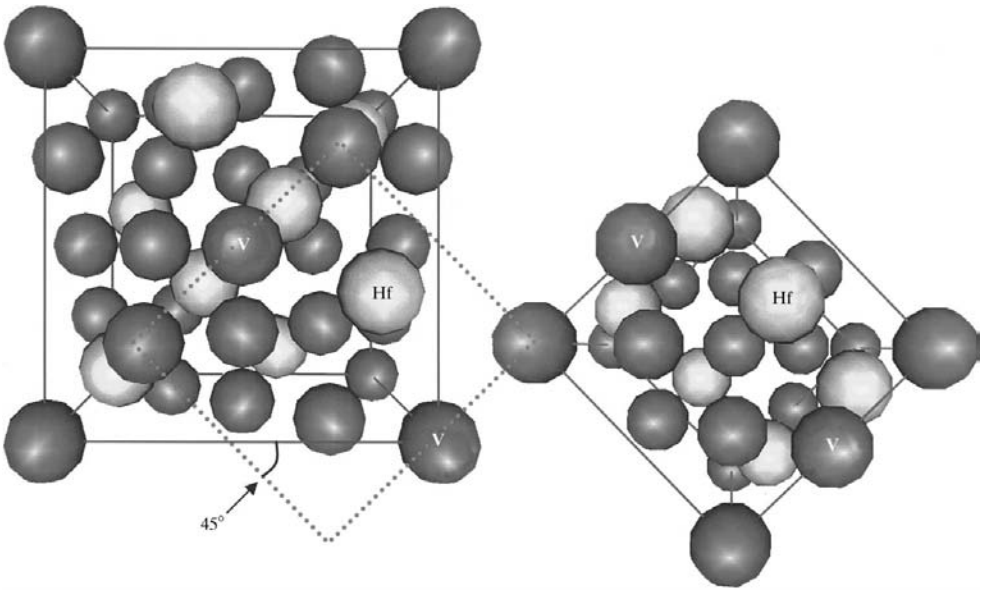

Figure 4
Atomic arrangement within the unit cell of HfV_2. The left side of the diagram shows the face-centered cubic (*Fd*3*m*) cell of $Z = 24$ and the right side shows the body-centered cell of $Z = 12$ in tetragonal ($I4_1/amd$) and orthorhombic (*Imma*) phases, respectively. The dashed frame illustrates the relationship between the unit cells of different structural phases, where the 45° rotation and $2^{1/2}$ reduction of the unit cell from cubic to lower symmetry phases are clearly shown.

diffraction profiles in terms of peak positions and peak intensities (Fig. 3), even for high 2θ angle (low *d*-spacing) diffraction peaks.

The unit cell of the tetragonal phase of $I4_1/amd$ is approximately half the cell volume with a 45° rotation in respect of the cubic *Fd*3*m* phase (Fig. 4). The unit cell of the tetragonal phase has the dimensions $a_T = b_T \simeq a_c/2^{1/2}$ and $c_T \simeq c_c$ compared with the cubic cell. The number of atoms in the unit cell also reduce from $Z = 24$ in the cubic phase to $Z = 12$ in the tetragonal phase, respectively. Further peak splitting observed below $T = 100$ K indicates a lower symmetry structure after the tetragonal phase.

3.2. Transition from tetragonal $I4_1/amd$ to orthorhombic *Imma*

The maximum non-isomorphic subgroups of the tetragonal $I4_1/amd$ phase are $I4_122$, $I4_1/a$, $I4_1md$, $I42d$, $I4m2$, *Imma* and *Fddd*, according to group theory. The first five of them are tetragonal phases and the last two are orthorhombic phases. We tested peak indexes and positions for two orthorhombic phases with the appropriate lattice parameters as the first step to resolve the crystal structure of the lower symmetry HfV_2 using the long-scan diffraction pattern collected at $T = 90$ K.

The orthorhombic *Fddd* ($Z = 24$) phase can match most peak positions for the diffraction pattern collected at $T = 90$ K, except for those peaks with an index of $h = k = l$ (same index and similar *d*-spacing as the cubic phase). These $h = k = l$ peaks of the cubic *Fd*3*m* ($Z = 24$) phase kept their singlet feature in the tetragonal $I4_1/amd$ ($Z = 12$) phase, but, however, split into doublets in the orthorhombic phase. The space group *Fddd* ($Z = 24$) failed to represent these new doublets and contradicted other systematic extinction rules in the experimental observation of the low-symmetry phase and thus was not the solution to the orthorhombic structure. The orthorhombic *Imma* ($Z = 12$) phase matched all peak positions for the diffraction pattern collected at $T = 90$ K. The intensity of the diffraction peak could also be fitted very nicely with the correct setting of structural parameters (atom positions) and thermal parameters. The diffraction pattern collected at $T = 20$ K could also be refined with the space group *Imma* ($Z = 12$) with adjusted lattice constants and structural parameters. Fig. 5 shows a selected section of the Rietveld refinement fit of diffraction patterns to illustrate the details of the structural phase transitions and corresponding peak changes. The averaged refinement statistics resulted in $\chi^2 = 8$–10 for four long-scan diffraction patterns, which is quite a good fit considering the large coverage of *d*-spacing from 0.75 to 8.55 Å and the many not-so-clean exclusions of the secondary mixture phase for the X-ray data.

3.3. Crystal structure of low-symmetry phases

As temperature cooled down across the transition temperature $T_{c1} = 112$ K, the atomic distances of the face-centered cubic phase adjusted correspondingly and resulted in the body-centered tetragonal phase. However, the orthorhombic *Imma* phase at temperatures below $T = 102$ K kept the body-centered feature and the same number of atoms in the unit cell ($Z = 12$) as the tetragonal $I4_1/amd$ phase.

Table 1 lists the structural and lattice parameters refined for cubic, tetragonal and orthorhombic phases, respectively.[1] Notice that our assignments of the atomic positions for both cubic *Fd*3*m* and orthorhombic *Imma* phases are different from Parsons *et al.* (1998). However, the resulting crystal structures of HfV_2 are identical. They may have a typographical error on the atomic position of V(2) in their orthorhombic *Imma* phase, where the 4(*d*) positions should be $\frac{1}{4}, \frac{1}{4}, \frac{3}{4}$, rather than $\frac{1}{4}, \frac{1}{4}, \frac{1}{4}$, otherwise the resulting bond lengths and angles could be very wrong. Using the structural and lattice parameters of Table 1 we calculated the bond lengths and angles for the cubic, tetragonal and orthorhombic phases of HfV_2. All the calcu-

[1] Supplementary data for this paper are available from the IUCr electronic archives (Reference: OS0043). Services for accessing these data are described at the back of the journal.

lated bond lengths and angles for different structural phases, as listed in Table 2, are consistent with small variations. The typical bond lengths are 2.61, 3.06 and 3.19 Å for V—V, V—Hf and Hf—Hf, respectively. The typical bond angles are 60, 120 and 180° for ⟨V—V—V⟩ and ⟨V—V—Hf⟩, respectively. While using Parsons *et al.*'s (1998) atomic position of V(2) at $\frac{1}{4}, \frac{1}{4}, \frac{1}{4}$ in the orthorhombic *Imma* phase, a Hf—V(2) bond length of 1.658 Å (unrealistically small!) would be obtained, plus more erroneous bond angles not consistent with the cubic *Fd3m* phase.

We could not observe the so-called 'untransformed cubic Laves phase' directly from the peak splitting of $(400)_C$. Contrary to Parsons *et al.*'s (1998) observation of triplet splitting, the $(400)_C$ peak in the cubic phase clearly split into two peaks $(220)_{T,O}$ and $(004)_{T,O}$ in the tetragonal and orthorhombic phases. Nevertheless, we tested their existence with the refinements for these long-scans diffraction data. On the positive side, the refinement results improved quite substantially, as indicated by the reduction of χ^2 by as much as 25–30%, with the introduction of a secondary 'untransformed cubic Laves phase'. However, the relative phase fractions for the 'untransformed cubic Laves phase' are way below the 33% value reported by Parsons *et al.* (1998). It is only ∼10–13% in our refinement results. Actually, the neutron diffraction employed in their experiment is not the correct technique to use to study HfV_2, because the neutron diffraction from the V atoms cannot be detected at all, owing to the near-zero coherent scattering length and significant incoherent scattering nature of the neutron.

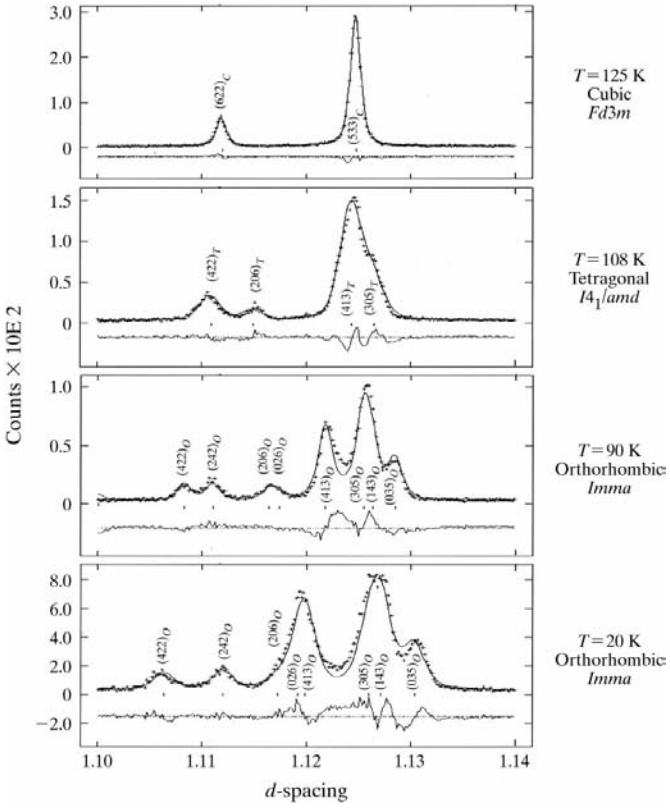

Figure 5
Refinement details for the cubic–tetragonal–orthogonal phase transitions. The diffraction data (*hkl*) are labeled next to the peaks with subscripts '$_C$', '$_T$' and '$_O$' to indicate the structural phases of cubic, tetragonal and orthorhombic, respectively.

3.4. Abnormal thermal expansion at low temperatures

In the tetragonal phase, the crystal structure of HfV_2 becomes distorted and the *a* axis of the cubic phase splits to a smaller *a* axis (contraction) and a longer *c* axis (expansion). As shown in Fig. 6 for a normalized (Z = 24) cell, the crystal-structure distortion of HfV_2 in the orthorhombic phase becomes more severe (indicated by further separation of the *a*, *b* and *c* axes) as temperature decreases. However, the cell volume shows apparent 'thermal contraction' in the low-symmetry phases. The atomic volume of HfV_2, *i.e.* the density of the material, decreases gradually with increasing temperature over the temperature range from 20 K to 100 K. Significant thermal contraction occurs in the temperature interval from 100 K to 115 K, where a whole sequence of *orthorhombic–tetragonal–cubic* phase transitions occur in the HfV_2 crystal structure. Phonon softening at the zone-center is

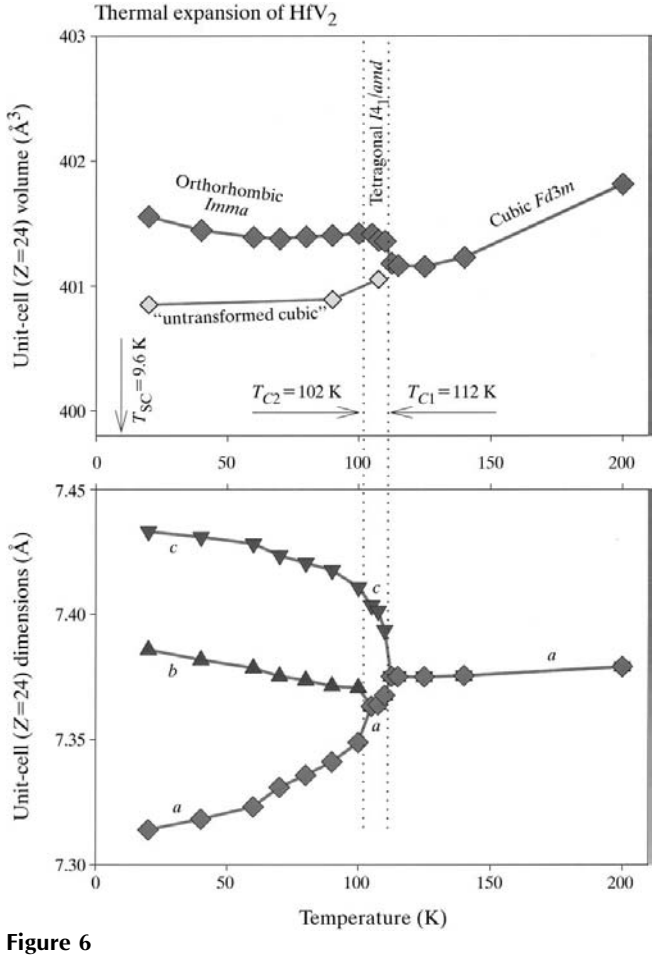

Figure 6
Unit-cell dimensions (normalized to Z = 24) plotted as a function of temperature. The abnormal thermal contraction within the tetragonal and orthorhombic phases can be clearly seen. Such an abnormality is mostly from the *b*-axis (in orthorhombic phase) and *c*-axis (in both orthorhombic and tetragonal phases) shrinkage over the temperature interval from 20 to 110 K. The 'untransformed cubic' is derived only for long-scan data.

Table 2
Selected geometric parameters (Å^2, °).

T = 125 K, Cubic *Fd3m*			
V—V^{i}	2.6075 (1)	Hf—Hf^{iii}	3.1935 (1)
V—Hf^{ii}	3.0576 (1)		

Symmetry codes: (i) $\frac{1}{4}+x,\frac{1}{4}+y,-z$; (ii) $\frac{1}{4}-z,x-\frac{1}{2},\frac{3}{4}-y$; (iii) $\frac{1}{4}+x,\frac{1}{4}+y,1-z$.

T = 108 K, Tetragonal $I4_1/amd$			
V—V^{i}	2.6102 (2)	V—Hf^{iii}	3.0544 (3)
V—V^{ii}	2.6036 (3)	Hf—Hf^{i}	3.1941 (3)
V—Hf	3.0657 (4)		

Symmetry codes: (i) $\frac{1}{4}-y,-\frac{1}{4}+x,\frac{1}{4}+z$; (ii) $-x,-\frac{1}{2}-y,z$; (iii) $\frac{1}{4}+y,\frac{1}{4}-x,z-\frac{1}{4}$.

Orthorhombic *Imma*		
	T = 90 K	T = 20 K
V1—V1^{i}	2.6062 (5)	2.6105 (6)
V1—V2^{ii}	2.6117 (2)	2.6132 (3)
V1—V2^{i}	2.6117 (2)	2.6132 (3)
V1—V2^{iii}	2.5955 (4)	2.5867 (5)
V1—Hf	3.0734 (3)	3.076 (2)
V1—Hf^{iv}	3.0481 (9)	3.0433 (7)
V1—Hf	3.0560 (9)	3.0573 (7)
V1—Hf^{v}	3.0677 (3)	3.074 (2)
Hf—Hf^{v}	3.1964 (4)	3.206 (3)
Hf—Hf^{iv}	3.1920 (4)	3.183 (3)

Symmetry codes: (i) $x,\frac{1}{2}-y,z$; (ii) $x,y-1,z$; (iii) $x,-\frac{1}{2}-y,z$; (iv) $\frac{1}{2}-x,\frac{1}{2}-y,\frac{1}{2}-z$; (v) $-x,1-y,1-z$.

considered to be the driving mechanism for the transition. Also plotted in Fig. 6 are the unit-cell volumes for the 'untransformed cubic' phase from the refinement results of three long-scan diffraction data at low temperatures. HfV_2 becomes superconducting at T_{sc} = 9.6 K (Chu *et al.*, 1996) and another orthorhombic phase *Imm*2 (a possible subgroup of *Imma*) has been reported at T = 6.0 K (Lawson & Zachariasen, 1972). Our refinement of diffraction data collected at T = 20 K indicate that the crystal structure of HfV_2 remains as the *Imma* phase. We have not reached the lower temperature and cannot confirm the structure.

4. Conclusions

We conclude that HfV_2 undergoes a series of structural transformations at low temperatures, not just one transition, in contrast to previous work. It transforms from a face-centered cubic (*Fd3m*) phase to a body-centered tetragonal ($I4_1/amd$) phase at 112 K and further transforms to a body-centered orthorhombic (*Imma*) phase at 102 K. HfV_2 seems to be always unstable with decreasing temperatures, as indicated by the continuous increase in the unit-cell volume (thermal contraction!). The structural refinements based on high-resolution synchrotron X-ray data provide accurate and precise atomic bond lengths and angles for each structural phase of HfV_2 at low temperatures.

We thank D. E. Cox and A. C. Lawson for helpful discussion. This work was partially performed under the auspices of the US Department of Energy under contract W-7405-ENG-36 with the University of California and by the Los Alamos Branch of the Institute of Geophysics and Planetary Physics. Work at Brookhaven was supported by the US Department of Energy, Division of Materials Sciences, under contract No. DE-AC02_76CH00016.

References

Balankin, A. S. & Skorov, D. M. (1982). *Sov. Phys. Solid State*, **24**, 681–682.
Chu, F., Chen, Z. W., Fuller, C. L., Lin, C. L. & Mihalisin, T. (1996). *J. Appl. Phys.* **79**, 6405–6407.
Chu, F., Lei, M., Migliori, A., Chen, S. P. & Mitchell, T. E. (1994). *Philos. Mag. B*, **70**, 867–880.
Chu, F. & Pope, D. P. (1993). *Mater. Sci. Eng. A*, **170**, 39–47.
Finlayson, T. R., Lanston, E. J., Simpson, M. A., Gibbs, E. E. & Smith, T. F. (1978). *J. Phys. F*, **8**, 2269–2278.
Hafstrom, J. W., Knapp, G. S. & Aldred, A. T. (1978). *Phys. Rev. B*, **17**, 2892–2900.
Larson, A. C. & Von Dreele, R. B. (1994). *GSAS Manual.* Los Alamos Unclassified Report LA-UR 86–748.
Lawson, A. C., Larson, A. C., Von Dreele, R. B., Ortiz, A. T., Smith, J. L., Faber, J., Hitterman, R. L. & Mueller, M. H. (1987). *J. Less-Common Met.* **132**, 229–235.
Lawson, A. C. & Zachariasen, W. H. (1972). *Phys. Lett. A*, **38**, 1.
Livingston, J. D. & Hall, E. L. (1990). *J. Mater. Res.* **5**, 5–8.
Parsons, M. J., Brown, P. J., Crangle, J., Neumann, K.-U., Ouladdiaf, B., Smith, T. J., Zayer, N. K. & Ziebeck, K. R. A. (1998). *J. Phys. Condens. Matter*, **10**, 8523–8534.
Rietveld, H. M. (1969). *J. Appl. Cryst.* **2**, 65–71.